Precision Microwave Spectroscopy of the Positronium $2\,^3S_1 \rightarrow 2\,^3P_2$ Interval

R. E. Sheldon, T. J. Babij, S. H. Reeder, S. D. Hogan, and D. B. Cassidy
Department of Physics and Astronomy, University College London, Gower Street, London WC1E 6BT, United Kingdom

(Received 14 April 2023; accepted 7 July 2023; published 27 July 2023)

We report the results of a new measurement of the positronium $2\,^3S_1 \rightarrow 2\,^3P_2$ (ν_2) interval. Using a modified experimental arrangement we have significantly reduced the effects of microwave reflections, which in previous experiments resulted in shifts and asymmetric line shapes. With the improved apparatus we obtain an experimental value of $\nu_2 = 8627.94 \pm 0.95$ MHz, which is within 1.3σ of the theoretical value 8626.71 ± 0.08 MHz.

DOI: 10.1103/PhysRevLett.131.043001

Precision spectroscopy of simple atomic systems can be used to test bound-state quantum electrodynamics (QED) theory and to measure fundamental constants [1]. In recent years such measurements, along with tests using more complex atomic and molecular systems, have also been employed for other fundamental physics applications, such as searches for new particles, dark matter, permanent electric dipole moments, and tests of discrete symmetries [2]. Some experiments in these areas make use of "exotic" atoms, which may have exaggerated or suppressed properties compared to their nonexotic counterparts. Exotic atoms may be loosely defined as hydrogenic atoms in which one or more particles has been replaced by an exotic analogue; common examples of such systems are muonium [3], muonic hydrogen [4], antihydrogen [5], and positronium (Ps) [6].

Of these exotic systems, Ps is the most easily produced, since positron beams can be obtained from radioactive sources [7], and do not require large accelerator facilities. Since Ps has no nuclear structure it is almost entirely described by QED, and is therefore a useful system with which to test bound-state QED theory, and also to search for physics not included in the standard model [8,9]. QED calculations of Ps energy levels have been completed up to $\mathcal{O}(m\alpha^6)$ [10,11], with some higher order terms obtained [12,13]. The theory precision is in all cases much higher than experimental results; for example, the ν_J intervals [$2\,^3S_1 \rightarrow 2\,^3P_J$ ($J = 0,\ 1,\ 2$)] have all been calculated with an estimated uncertainty of 80 kHz, while the corresponding experimental uncertainties have been > 1 MHz for 30 yr [14–16]. New measurements of these intervals have achieved improved precision, but asymmetric line shapes obtained for the ν_1 and ν_2 transitions prevented accurate identification of the transition frequencies [17]. Furthermore, measurements of the ν_0 transition presented an apparent discrepancy with theory [6].

We report here a new measurement of the ν_2 transition using a modified experimental apparatus designed to resolve these problems. This transition was chosen because it is the strongest of the fine structure transitions, and was previously observed to be asymmetric. Numerical simulations [18] and free-space microwave spectroscopy [19] have indicated that microwave reflections in the vacuum chamber were responsible for the previously observed asymmetric line shapes, and may also have given rise to apparent frequency shifts, without causing measurable asymmetry. Based on these studies, we have reconfigured the experimental apparatus to reduce or eliminate reflections, and to provide improved control over other systematic effects.

The methods used in the experiments we describe here are similar to those used in previous work [17]. A Surko-type positron trap [20] was used to generate Ps atoms by implanting a 3 ns, 3 mm (FWHM) positron pulse [21] into a porous silica film [22]. Ps atoms in the 1^3S_1 ground state were then emitted from this film with transverse kinetic energies on the order of 50 meV [23], and were excited to $n = 2$ states using a pulsed ultraviolet (UV) dye laser ($\lambda = 243$ nm, $\Delta\nu = 100$ GHz, $\Delta t = 4$ ns) [21]. Ps atoms in the 2^3S_1 state were produced using a Stark-mixing excitation scheme described in detail elsewhere [24]; laser excitation was performed in an electric field of 4 kV/cm, which was turned off within 25 ns to allow pure 2^3S_1 atoms to propagate in zero field into a WR-112 waveguide, as shown in Fig. 1. In the waveguide $2\,^3S_1 \rightarrow 2\,^3P_2$ transitions were driven by microwave radiation propagating in either the $+x$ or $-x$ directions. The rectangular waveguide only allows TE_{10} modes to propagate, and only the z component of the electric field is nonzero. This means that only transitions for

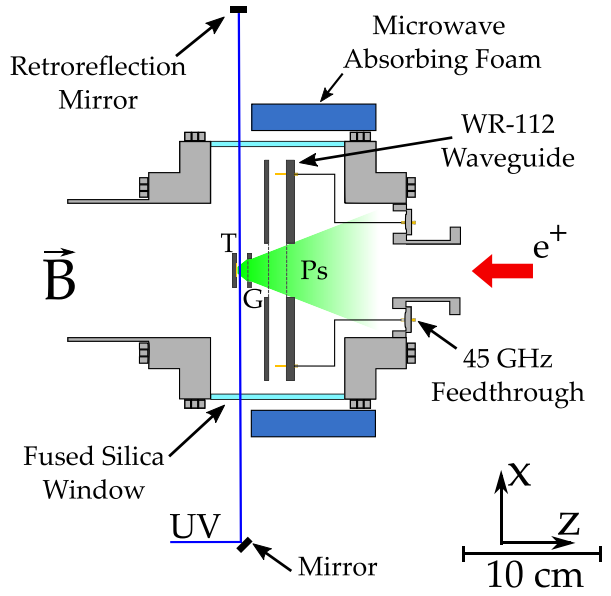

FIG. 1. Schematic representation of the target chamber and waveguide. Ps atoms produced by positron implantation in a target electrode (T), were optically excited to the $2\,^3S_1$ level and passed through a waveguide via high transmission (95%) grids. Ps annihilation radiation was measured using γ-ray detectors placed around the chamber (not shown).

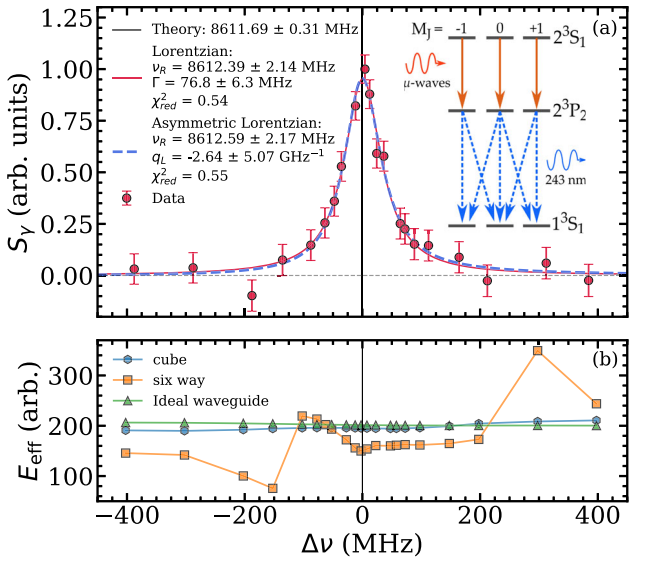

FIG. 2. (a) Spectral line shape with both symmetric (solid red line) and asymmetric (dashed blue line) fits, as described in the text. The corresponding fit parameters and reduced chi square values are indicated in the legend. These data were recorded in a magnetic field of 97 G with the microwave radiation incident from the $-x$ direction, and the solid vertical line represents the calculated value for the transition frequency in this field. The inset shows the allowed transitions with stimulated (solid orange arrows) and radiative (dashed blue arrows) decay pathways. (b) Numerical simulations of the electric field in the waveguide for different experimental configurations (the lines joining points are to guide the eye only).

which $\Delta M_J = 0$ were driven [17], where M_J represents the z projection of the total angular momentum $\vec{J}$.

Microwave induced transitions were detected via changes in the time spectrum of Ps annihilation radiation [25], measured using γ-ray detectors comprising a lutetium-yttrium oxyorthosilicate scintillator attached to a photomultiplier tube [26]. Four separate gamma-ray detectors were placed around the vacuum chamber. These were used to record single-shot lifetime spectra [27]. Atoms driven to the $2\,^3P_2$ level decay to the 1^3S_1 ground state in 3.2 ns, and since the decay rate of $2\,^3S_1$ atoms is 8 times lower than that of 1^3S_1 atoms [9], such transitions can be detected via changes in Ps lifetime spectra. These were characterized by the signal parameter S_γ (see Ref. [17] for details), and line shapes were generated by measuring S_γ as a function of the microwave frequency. An example line shape measured in this way is shown in Fig. 2(a). The reduced chi square values (χ^2_{red}) for the entire dataset generally vary from $\approx$ 0.5–1.5.

In previous experiments asymmetric line shapes were characterized using a Fano function [17]. Here this approach was less useful because the degree of asymmetry was much reduced, and line shape asymmetry was characterized using an asymmetric Lorentz function [28], as described in Ref. [19]. In this formalism, the Lorentzian width Γ_L is replaced with a function of the form $\Gamma_A(\nu) = 2\Gamma_L/\{1 + \exp[q(\nu - \nu_R)]\}$, where q is an asymmetry parameter such that in the limit $q \to 0$, the asymmetric function approaches a standard Lorentzian function. The data shown in Fig. 2 have been fitted to both symmetric and asymmetric Lorentz functions; these fits yield the same ν_R results (within errors), as was the case for all measured line shapes. The average q values obtained for all measurements are shown in Table I. For comparison, the previous ν_2 measurements performed in the larger six-way vacuum chamber [17] yielded an average value of $q = 23.2 \pm 0.5$ GHz^{-1}; the present values for q are considerably smaller than this.

TABLE I. Measured values for the parameters q, a, and ν_2 for different microwave propagation directions $\pm x$. ν_2^A refers to fits made using an asymmetric Lorentz function, and $[F]$ denotes the presence of microwave absorbing foam, as described in the text.

	$+x$	$-x$
q (GHz^{-1})	-4.5 ± 0.7	-2.2 ± 0.7
q $[F]$ (GHz^{-1})	-6.7 ± 0.7	-2.7 ± 0.9
a (kHz/G^2)	-1.65 ± 0.06	-1.67 ± 0.06
a $[F]$ (kHz/G^2)	-1.71 ± 0.07	-1.63 ± 0.09
ν_2 (MHz)	8628.97 ± 0.53	8626.77 ± 0.59
ν_2^A (MHz)	8629.15 ± 0.55	8626.81 ± 0.61
ν_2 $[F]$ (MHz)	8628.29 ± 0.66	8627.03 ± 0.69
ν_2^A $[F]$ (MHz)	8628.63 ± 0.70	8627.26 ± 0.71

Numerical simulations of the microwave field in the new experimental arrangement were performed (see Ref. [18] for details). Variations in the average electric field in the waveguide were obtained as a function of frequency in the x-y plane along the center of the waveguide. Figure 2(b) shows the fields calculated for the old and new configurations, as well as that of an ideal waveguide. These data support the expectation that the cubic chamber is less susceptible to reflections than the previous vacuum chamber, and thus explain why the line shapes observed in the present case are more symmetric than those observed in the previous ν_2 measurements [17].

The experiments we describe here were conducted in an axial magnetic field B, which is necessary for the operation of the positron trap [20]. This means that the measured transition frequencies were Zeeman shifted [29]; to account for this we measured $\nu_R(B)$, the Zeeman-shifted transition frequencies, for different magnetic fields, and extrapolated these measurements to find the zero-field value (i.e., ν_2). The magnetic field strength in the measurement chamber could be varied from 40–125 G. This field, including any residual fields not generated by the magnets, was measured with a hall probe accurate to 1%. Variations in the magnetic field in the waveguide region were found to be below ± 1 G. This was used as the error in B in the fits and was found to have a negligible effect.

The measured and calculated Zeeman shifted transition frequencies are shown in Fig. 3. Each ν_R data point is the average of those obtained from four individual detectors, and measurements were performed with the microwave radiation propagating in the $+x$ and $-x$ directions, as indicated in the figure. Because of the low magnetic fields used in the experiment, the quadratic Zeeman shift

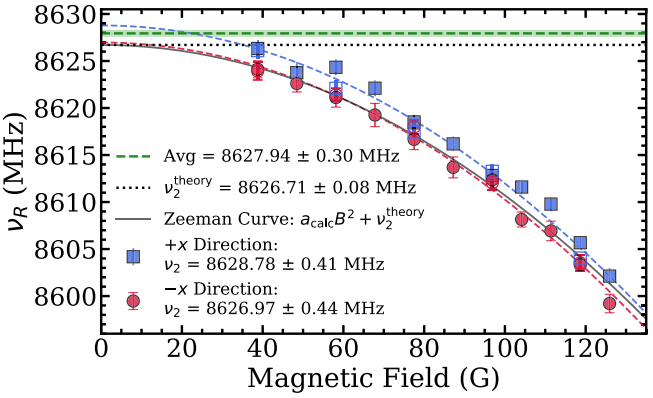

FIG. 3. ν_R transition frequency measured for different magnetic fields. The blue squares represent microwave propagation in the $+x$ direction and the red circles in the $-x$ direction. Open points were obtained with microwave absorbing foam on the windows. The solid and dashed gray lines are the calculated Zeeman shift and zero-field frequencies, respectively. The dashed (red and blue) curves are fits to the data ($\chi^2_{\text{red}} = 2.18$ and 0.62, respectively). The dashed green line is the average of the ν_2 values.

dominates [30], and the data were fitted to a function of the form $\nu_R = aB^2 + c$, using an orthogonal distance regression package in PYTHON [31]. The intercept c corresponds to the field-free transition frequency ν_2 and the error in B was ± 1 G. The obtained values for ν_2 are shown in Table I, where the reported errors are statistical only. The a coefficients obtained from the fits are also shown in Table I. As the ν_2 transition includes two different transitions between different substates (see inset to Fig. 2), the theoretical curve shown in Fig. 3 has been calculated using a weighted average based on the individual transition strengths. From this the theoretical value of the a coefficient is $a_{\text{calc}} = -1.60$ kHz/G^2 which is largely consistent with the measured values shown in Table I.

The main changes in the current experiment are that we have (1) reduced microwave reflections using a different vacuum chamber, (2) reversed the direction of the microwave radiation, (3) retroreflected the excitation laser beam, and, (4) added a grounded grid between the target electrode and the waveguide. The grounded grid (the G electrode in Fig. 1) was installed in case the target potential varied during the measurement. Previously the waveguide itself was used as the ground plane for the excitation electric field. The $2\,^3S_1$ production method [24] involves rapidly switching off an electric field, and we have found that the high-voltage switch used to do this can ring at a low level, meaning that there was a possibility that a small electric field might have been induced in the waveguide during the measurements. Although the magnitude of any such fields was expected to be negligible, the additional grid was installed as a precaution.

Retroreflection of the UV excitation laser was implemented to counteract any effects that might arise from laser wavelength drifts during the measurements. Although Doppler profiles of the $1\,^3S_1 \rightarrow 2\,^3P_J$ transition were measured between runs, the laser frequency was not monitored continuously, and so the overall stability during the measurements was not known. The retroreflected beam also removes the recoil effect arising from excitation with a single beam exactly on resonance [17].

The most significant improvement in the experiment was the reduction of reflected microwave radiation. In previous experiments the ν_2 transition was found to be highly asymmetric [17], to the extent that line shape fitting using symmetric and asymmetric functions resulted in inferred transition frequencies that differed by several MHz. Subsequent simulations [18] and free-space measurements [19] indicated that this was likely due to a frequency dependence in reflected microwave radiation entering the waveguide. The new experiments were performed in a cubic vacuum chamber in which the waveguide extended to within 1 cm of a large fused silica vacuum window, as shown in Fig. 1. This window is expected to have a very low reflection coefficient for microwave radiation, and also allows the UV excitation

laser to enter the vacuum chamber without introducing additional reflective elements.

Additionally, measurements were taken with and without broadband microwave absorbing foam (Eccosorb-AN [32]) mounted near the windows (see Fig. 1) with a nominal reflectivity of −25 dBm in the relevant frequency range. With the exception of some asymmetry q values (see Table I), no difference was observed between data taken with and without the foam (see Table I), supporting the prior conclusion that reflected microwave radiation effects in the cube geometry are negligible.

Reversing the reversed the direction of propagation radiation takes into account any Doppler shifts arising from a possible misalignment of the excitation laser path with the axis of the waveguide. We estimate that the misalignment could be at most 5°, and using trajectory simulations we determined that associated Doppler shifts would be less than 250 kHz. The separation of the incident and reflected laser beams after a 1 m flight path indicated that the angle between them was less than 0.6°.

As shown in Table I, the transition frequencies obtained from fits using symmetric and asymmetric Lorentz functions were identical (within errors); the average value obtained from asymmetric Lorentz fits (for both microwave directions) was $\nu_2^A = 8628.12 \pm 0.31$ MHz, which differs from the symmetric case by only 0.14 MHz. In free-space experiments, shifts on the order of 10 MHz were observed by rotating the horn antenna used to generate the microwave radiation. However, the corresponding line shapes did not exhibit any significant asymmetry ($q = -0.54 \pm 0.56\ \mathrm{GHz}^{-1}$) [19]. We conclude from this that, within our current statistical uncertainty, symmetric line shapes do not necessarily indicate that the measurements are free from perturbing effects.

The final result is obtained from the average value of the measurements made for each microwave direction (see Fig. 3). Fits were made in each case using all data points (i.e., with and without the microwave absorbing foam); the average value obtained is $\nu_2 = 8627.94 \pm 0.30$ MHz. We note that we obtain almost the same result (8627.75 ± 0.27 MHz) if the data are averaged at each field and then fitted. A comparison of this result with previous measurements of the same interval is shown in Fig. 4.

The systematic effects in the current work are similar to those of previous measurements, except we have eliminated Doppler shifts arising from possible laser misalignment or laser wavelength drifts. Other effects, such as stray electric fields, ac Stark shifts, or motional Stark shifts are expected to contribute less than 10 kHz to the total uncertainty budget [17]. Detailed simulations indicate that misalignment of the magnetic field could cause Lorentz fits to be shifted by 32 kHz (for a 10° tilt) [18].

The impact of quantum interference (QI) effects of the type arising from neighboring resonances (e.g., [33–35]) has been calculated explicitly for our experimental arrangements [18]. We found that QI shifts depend on the orientation of the gamma-ray detectors and the degree of saturation of the transition, but for realistic experimental parameters give rise to errors in the measured transition frequency of less than 30 kHz. Since the *individual* line shapes exhibited fitting errors on the order of 1 MHz [e.g., Fig. 2(a)] it was not feasible to fit the data using a line shape that explicitly included the QI perturbations (e.g., as in Ref. [36]). We therefore used standard Lorentz functions to fit our line shapes, and include QI effects as a systematic error in the present measurements. As a conservative estimate we take the total systematic error contribution due to QI and all Stark and Zeeman effects in the experiment to be 100 kHz.

It is evident from the data shown in Fig. 3 that there is a significant difference between the ν_2 values obtained for the $+x$ and $-x$ cases, amounting to 1.8 MHz. This difference is too large to be caused by Doppler shifts, which contribute less than 0.5 MHz. Since we obtain two different results from nominally identical arrangements we conclude that there exists an additional intrinsic systematic effect occurring via a physical mechanism in the waveguide that is distinct from the reflected radiation effect previously identified. Conti and co-workers have suggested that, in a waveguide similar to that used here, standing waves with nodes located over the mesh covered holes could be present [37]. If the shape of the transmission meshes affects such waves then a directional asymmetry could arise from corresponding asymmetric mesh properties. S-parameter measurements (S_{12} and S_{21} [38]) using a network analyzer (Agilent N5224A) were performed to test this, but no significant difference between the two directions was observed. It is possible that different radiation field distributions exist within the waveguide for different propagation directions, even if the power transmission, and hence the S parameters, remain the same. In the absence of a qualitative model we cannot conclusively rule out an effect of this type.

We expect that, at most, 0.5 MHz of the 1.8 MHz difference between the $\pm x$ measurements can be attributed

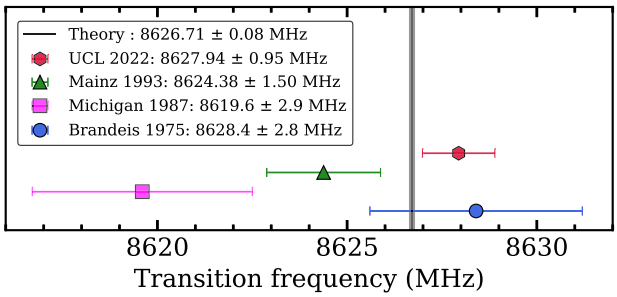

FIG. 4. Measurements of the $2\,^3S_1 \rightarrow 2\,^3P_2$ interval over almost 50 years, obtained by groups from Brandeis [14], Michigan [15], Mainz [16], and the present work (UCL 2022). Where available, systematic and statistical errors have been added in quadrature. The vertical line represents the theory value, taken from Ref. [11].

to Doppler shifts caused by laser misalignment (i.e., 0.25 MHz in each direction). We take account of the observed difference using an associated systematic error of $1.8/2 = 0.9$ MHz. Including this makes our final result $\nu_2 = 8627.94 \pm 0.30_{\text{stat}} \pm 0.91_{\text{sys}}$ MHz. This differs from the theoretical value by 1.23 MHz, or 1.3σ.

The precision of the current measurement is dominated by an unknown systematic effect that appears to be an intrinsic property of the waveguide, possibly connected to the (unavoidable) use of meshes. This kind of effect may be reduced by using an improved waveguide design, but may also be mitigated by using a different approach, in which it is not necessary to scan the microwave radiation frequency over several hundred MHz, as is dictated by the (50 MHz) natural width of the transition. This may be accomplished by using the Ramsey method of separated oscillatory fields [39,40], and in particular the frequency offset separated oscillatory field (FOSOF) technique developed by Hessels and co-workers [41]. FOSOF measurements are not sensitive to the full frequency response of the system, and should therefore be free of many of the limitations of the present measurement techniques. However, slow Ps atoms do not live long enough to pass between separated field regions, and a Ps FOSOF measurement will require the development of a fast 2^3S_1 Ps beam [42]; an experiment along these lines is currently being constructed [43].

We gratefully acknowledge L. Liszkay for providing silica samples, and J. Dumper, F. Noyes, and R. Jawad for technical assistance. This work was supported by the EPSRC under Grant No. EP/W032023/1.

[1] S. G. Karshenboim, Precision physics of simple atoms: QED tests, nuclear structure and fundamental constants, Phys. Rep. **422**, 1 (2005).
[2] M. S. Safronova, D. Budker, D. DeMille, Derek F. Jackson Kimball, A. Derevianko, and C. W. Clark, Search for new physics with atoms and molecules, Rev. Mod. Phys. **90**, 025008 (2018).
[3] B. Ohayon, G. Janka, I. Cortinovis, Z. Burkley, L. de Sousa Borges, E. Depero, A. Golovizin, X. Ni, Z. Salman, A. Suter, C. Vigo, T. Prokscha, and P. Crivelli (Mu-MASS Collaboration), Precision Measurement of the Lamb Shift in Muonium, Phys. Rev. Lett. **128**, 011802 (2022).
[4] R. Pohl, R. Gilman, G. A. Miller, and K. Pachucki, Muonic hydrogen and the proton radius puzzle, Annu. Rev. Nucl. Part. Sci. **63**, 175 (2013).
[5] M. Ahmadi *et al.*, Characterization of the 1s-2s transition in antihydrogen, Nature (London) **557**, 71 (2018).
[6] L. Gurung, T. J. Babij, S. D. Hogan, and D. B. Cassidy, Precision Microwave Spectroscopy of the Positronium $n = 2$ Fine Structure, Phys. Rev. Lett. **125**, 073002 (2020).
[7] P. G. Coleman, *Positron Beams and Their Applications*, 1st ed. (World Scientific Publishing Co., Singapore, 2000).
[8] S. G Karshenboim, Precision study of positronium: Testing bound state QED theory, Int. J. Mod. Phys. A **19**, 3879 (2004).
[9] G. S. Adkins, D. B. Cassidy, and J. Pérez-Ríos, Precision spectroscopy of positronium: Testing bound-state QED theory and the search for physics beyond the standard model, Phys. Rep. **975**, 1 (2022).
[10] Andrzej Czarnecki, Kirill Melnikov, and Alexander Yelkhovsky, Positronium S-state spectrum: Analytic results at $o(m\alpha^6)$, Phys. Rev. A **59**, 4316 (1999).
[11] Andrzej Czarnecki, Kirill Melnikov, and Alexander Yelkhovsky, Positronium Hyperfine Splitting: Analytical Value at $o(m\alpha^6)$, Phys. Rev. Lett. **82**, 311 (1999).
[12] G S Adkins, Higher order corrections to positronium energy levels, J. Phys. Conf. Ser. **1138**, 012005 (2018).
[13] Michael I. Eides and Valery A. Shelyuto, Three-loop corrections to the lamb shift in muonium and positronium, Phys. Rev. A **105**, 012803 (2022).
[14] A. P. Mills, Jr., S. Berko, and K. F. Canter, Fine-Structure Measurement in the First Excited State of Positronium, Phys. Rev. Lett. **34**, 1541 (1975).
[15] S. Hatamian, R. S. Conti, and A. Rich, Measurements of the 2^3S_1-2^3P_J ($J = 0$, 1, 2) Fine-Structure Splittings in Positronium, Phys. Rev. Lett. **58**, 1833 (1987).
[16] D. Hagena, R. Ley, D. Weil, G. Werth, W. Arnold, and H. Schneider, Precise Measurement of $n = 2$ Positronium Fine-Structure Intervals, Phys. Rev. Lett. **71**, 2887 (1993).
[17] L. Gurung, T. J. Babij, J. Pérez-Ríos, S. D. Hogan, and D. B. Cassidy, Observation of asymmetric line shapes in precision microwave spectroscopy of the positronium $2^3s_1 \rightarrow 2^3p_J$ ($j = 1, 2$) fine-structure intervals, Phys. Rev. A **103**, 042805 (2021).
[18] L. A. Akopyan, T. J. Babij, K. Lakhmanskiy, D. B. Cassidy, and A. Matveev, Line-shape modeling in microwave spectroscopy of the positronium $n = 2$ fine-structure intervals, Phys. Rev. A **104**, 062810 (2021).
[19] R. E. Sheldon, T. J. Babij, S. H. Reeder, S. D. Hogan, and D. B. Cassidy, Microwave spectroscopy of positronium atoms in free space, Phys. Rev. A **107**, 042810 (2023).
[20] J. R. Danielson, D. H. E. Dubin, R. G. Greaves, and C. M. Surko, Plasma and trap-based techniques for science with positrons, Rev. Mod. Phys. **87**, 247 (2015).
[21] B. S. Cooper, A. M. Alonso, A. Deller, T. E. Wall, and D. B. Cassidy, A trap-based pulsed positron beam optimised for positronium laser spectroscopy, Rev. Sci. Instrum. **86**, 103101 (2015).
[22] L. Liszkay, C. Corbel, P. Perez, P. Desgardin, M. F. Barthe, T. Ohdaira, R. Suzuki, P. Crivelli, U. Gendotti, A. Rubbia, M. Etienne, and A. Walcarius, Positronium reemission yield from mesostructured silica films, Appl. Phys. Lett. **92**, 063114 (2008).
[23] D. B. Cassidy, P. Crivelli, T. H. Hisakado, L. Liszkay, V. E. Meligne, P. Perez, H. W. K. Tom, and A. P. Mills, Jr., Positronium cooling in porous silica measured via Doppler spectroscopy, Phys. Rev. A **81**, 012715 (2010).
[24] A. M. Alonso, S. D. Hogan, and D. B. Cassidy, Production of 2^3S_1 positronium atoms by single-photon excitation in an electric field, Phys. Rev. A **95**, 033408 (2017).
[25] David B. Cassidy, Experimental progress in positronium laser physics, Eur. Phys. J. D **72**, 53 (2018).

[26] A. M. Alonso, B. S. Cooper, A. Deller, and D. B. Cassidy, Single-shot positron annihilation lifetime spectroscopy with LYSO scintillators, Nucl. Instrum. Methods Phys. Res., Sect. A **828**, 163 (2016).
[27] D. B. Cassidy, S. H. M. Deng, H. K. M. Tanaka, and A. P. Mills, Jr., Single shot positron annihilation lifetime spectroscopy, Appl. Phys. Lett. **88**, 194105 (2006).
[28] Aaron L. Stancik and Eric B. Brauns, A simple asymmetric lineshape for fitting infrared absorption spectra, Vib. Spectrosc. **47**, 66 (2008).
[29] A. M. Alonso, B. S. Cooper, A. Deller, S. D. Hogan, and D. B. Cassidy, Controlling Positronium Annihilation with Electric Fields, Phys. Rev. Lett. **115**, 183401 (2015).
[30] M. L. Lewis and V. W. Hughes, Higher-order relativistic contributions to the combined Zeeman and motional Stark effects in positronium, Phys. Rev. A **8**, 625 (1973).
[31] Guido Van Rossum and Fred L. Drake, *Python 3 Reference Manual* (CreateSpace, Scotts Valley, CA, 2009).
[32] Microwave absorbing foams, Https://www.laird.com/products/microwave-absorbers/microwave-absorbing-foams.
[33] M. Horbatsch and E. A. Hessels, Shifts from a distant neighboring resonance, Phys. Rev. A **82**, 052519 (2010).
[34] M. Horbatsch and E. A. Hessels, Shifts from a distant neighboring resonance for a four-level atom, Phys. Rev. A **84**, 032508 (2011).
[35] Thomas Udem, Lothar Maisenbacher, Arthur Matveev, Vitaly Andreev, Alexey Grinin, Axel Beyer, Nikolai Kolachevsky, Randolf Pohl, Dylan C. Yost, and Theodor W. Hänsch, Quantum interference line shifts of broad dipole-allowed transitions, Ann. Phys. (Berlin) **531**, 1900044 (2019).
[36] Axel Beyer, Lothar Maisenbacher, Arthur Matveev, Randolf Pohl, Ksenia Khabarova, Alexey Grinin, Tobias Lamour, Dylan C. Yost, Theodor W. Hänsch, Nikolai Kolachevsky, and Thomas Udem, The rydberg constant and proton size from atomic hydrogen, Science **358**, 79 (2017).
[37] R. S. Conti, S. Hatamian, L. Lapidus, A. Rich, and M. Skalsey, Search for C-violating, P-conserving interactions and observation of 2^3S_1 to 2^1P_1 transitions in positronium, Phys. Lett. A **177**, 43 (1993).
[38] David M. Pozar, *Microwave Engineering*, 4th ed. (Wiley, Hoboken, NJ, 2012).
[39] Norman F. Ramsey, A new molecular beam resonance method, Phys. Rev. **76**, 996 (1949).
[40] Norman F. Ramsey, Experiments with separated oscillatory fields and hydrogen masers, Rev. Mod. Phys. **62**, 541 (1990).
[41] A. C. Vutha and E. A. Hessels, Frequency-offset separated oscillatory fields, Phys. Rev. A **92**, 052504 (2015).
[42] N. Bezginov, T. Valdez, M. Horbatsch, A. Marsman, A. C. Vutha, and E. A. Hessels, A measurement of the atomic hydrogen lamb shift and the proton charge radius, Science **365**, 1007 (2019).
[43] T. J. Babij and D. B. Cassidy, Positronium microwave spectroscopy using Ramsey interferometry, Eur. Phys. J. D **76**, 121 (2022).